

2 **Measurement of mixing-induced CP violation Using Partial**
3 **Reconstruction of $\bar{B}^0 \rightarrow D^{*+} X \ell^- \bar{\nu}_\ell$ and Kaon Tag.**

4 The *BABAR* Collaboration

5 Enrico Feltresi, Martino Margoni, Franco Simonetto
6 INFN and Universita' di Padova, Italy.
7

8 August 28, 2012

9 **Abstract**

10 We present a new measurement of CP violation induced by $B^0 \bar{B}^0$ oscillation, based on the full
11 data set collected by the *BABAR* experiment at the PEP-II collider. We apply an original technique
12 to a sample of about 5 million $\bar{B}^0 \rightarrow D^{*+} \ell^- \bar{\nu}_\ell$ decays reconstructed with partial reconstruction
13 of the D^{*+} meson. The charged lepton identifies the flavor of the first B meson at its decay
14 time, the flavor of the other B is determined by Kaon tagging. We determine the parameter
15 $\delta = 1 - |q/p| = (0.29 \pm 0.84_{-1.78}^{+1.60}) \times 10^{-3}$. The precision of this measurement is comparable to that
16 obtained by B-factories with dilepton samples.

17 1 Introduction

18 The effective Hamiltonian which describes mixing and decay of B^0 mesons is written in terms of
 19 2×2 hermitian matrices: $\mathbf{H} = \mathbf{M} - i/2\mathbf{\Gamma}$. The two mass eigenstates of the Hamiltonian, carrying
 20 mass m_L and m_H , are expressed in terms of the flavor eigenstates, B^0 and \bar{B}^0 , as:

$$\begin{aligned} |B_L\rangle &= p|B^0\rangle + q|\bar{B}^0\rangle \\ |B_H\rangle &= p|B^0\rangle - q|\bar{B}^0\rangle. \end{aligned}$$

21 Any deviation from unity of the ratio $|q/p|$ would imply that the mass eigenstates are not CP
 22 eigenstates, which would result in the so-called CP violation in mixing. The value of $|q/p|$ is
 23 computed in terms of the off diagonal matrix elements. In the Standard Model, a number very
 24 next to unity is expected: one of the most recent theoretical calculations [1], including NLO QCD
 25 corrections, predicts:

$$\delta_{CP} = 1 - |q/p| = -(2.96 \pm 0.67) \times 10^{-4}.$$

26 A sizeable deviation from unity would be a clear proof of New Physics beyond the Standard Model.
 27 If CP is violated in Mixing, the probability of a B^0 to oscillate to a \bar{B}^0 is different from the
 28 probability of a \bar{B}^0 to oscillate to a B^0 and thus we expect to observe a different number of $B^0 B^0$
 29 events with respect to $\bar{B}^0 \bar{B}^0$. A value different from 0 is then expected for the dilepton asymmetry,
 30 defined as:

$$\mathcal{A}_{\ell\ell} = \frac{N(B^0 B^0) - N(\bar{B}^0 \bar{B}^0)}{N(B^0 B^0) + N(\bar{B}^0 \bar{B}^0)} = \frac{N(\ell^+ \ell^+) - N(\ell^- \ell^-)}{N(\ell^+ \ell^+) + N(\ell^- \ell^-)} \simeq 2\delta_{CP}, \quad (1)$$

31 where we neglect background and detector related charge asymmetries in lepton identification.

32 The Belle [2] and BABAR [3] Collaborations presented results based on the analysis of events
 33 with two identified leptons (dilepton events). The $D\theta$ Collaboration [4] obtained a more precise
 34 measurement with a dimuon sample, which however includes contributions from B^0 and B_s mixing.
 35 They observe a deviation larger than three standard deviations from the SM expectation. An
 36 analysis of the muon impact parameters attributes the effect to B_s mesons. A recent measurement
 37 of LHCb [5] based on the reconstruction of $\bar{B}_s \rightarrow D_s^{(*)+} \ell^- \bar{\nu}_\ell$ decays is compatible both with the SM
 38 and with $D\theta$.

39 The dilepton measurements benefit from the large amount of events which can be selected at
 40 B-factories or at hadron colliders. They however rely on the use of control samples to subtract the
 41 charge asymmetric background from hadron to lepton misidentification or light hadron decay, and
 42 to compute the charge dependent lepton identification asymmetry which may produce a fake signal.
 43 These systematic uncertainties constitute a severe limitation to the precision of the measurement.

44 We present here a new kind of measurement. We partially reconstruct $\bar{B}^0 \rightarrow D^{*+} \ell^- \bar{\nu}_\ell$ decays by
 45 identifying only the charged lepton and the low momentum pion (π_s) from the $D^{*+} \rightarrow D^0 \pi_s$ decays.
 46 A state decaying as a B^0 (\bar{B}^0) meson produces a positive (negative) charge lepton. Neglecting higher
 47 order terms, the observed asymmetry between the number of positive-charge and negative-charge
 48 leptons is therefore:

$$A_\ell \simeq \mathcal{A}_{rec,\ell} + \mathcal{A}_{\ell\ell} \cdot \chi_d, \quad (2)$$

49 where $\chi_d = 0.1862 \pm 0.0023$ [6] is the integrated mixing probability for B^0 mesons, and $\mathcal{A}_{rec,\ell}$ is
 50 the charge asymmetry in the reconstruction of $\bar{B}^0 \rightarrow D^{*+} \ell^- \bar{\nu}_\ell$ decays.

51 We use Kaons from the decays of the other B^0 hadrons to tag its flavor (K_T). A state decaying
 52 as a B^0 (\bar{B}^0) meson results most often in a $K^+(K^-)$. If mixing takes place, the ℓ and the K have
 53 then the same electric charge. In the same approximations as before, the observed asymmetry in
 54 the rate of mixed events is:

$$A_{mix} = \frac{N(\ell^+ K_T^+) - N(\ell^- K_T^-)}{N(\ell^+ K_T^+) + N(\ell^- K_T^-)} \simeq \mathcal{A}_{rec,\ell} + \mathcal{A}_{tag} + \mathcal{A}_{\ell\ell}, \quad (3)$$

55 where \mathcal{A}_{tag} is the charge asymmetry in K reconstruction. A Kaon with the same charge as the ℓ
 56 might also come from the Cabibbo Favored (CF) decays of the D^0 meson produced with the lepton
 57 from the partially reconstructed side (K_R). The asymmetry observed for these events is then:

$$A_{same} = \frac{N(\ell^+ K_R^+) - N(\ell^- K_R^-)}{N(\ell^+ K_R^+) + N(\ell^- K_R^-)} \simeq \mathcal{A}_{rec,\ell} + \mathcal{A}_{tag} + \mathcal{A}_{\ell\ell} \cdot \chi_d \quad (4)$$

58 Equations 2,3, and 4 can be inverted to extract $\mathcal{A}_{\ell\ell}$ and the detector induced asymmetries. It is
 59 not possible to distinguish in each event a K_T from a K_R . They are separated on statistical basis,
 60 using kinematics features and proper time difference information. We perform a multidimensional
 61 binned-likelihood fit to determine, together with the asymmetries, several other factors which would
 62 be otherwise sources of systematic uncertainty.

63 The *BABAR* detector is described briefly in the next section. Event selection, sample composition
 64 and B-flavor tagging is then described in Sec.3. The measurement of $\mathcal{A}_{\ell\ell}$ is described in Sec.4, the
 65 discussion of the systematic uncertainties follows in Sec.5, while we summarize the results and draw
 66 our conclusions in Sec.6.

67 2 The *BABAR* Detector

68 The data sample used in this analysis consists of an integrated luminosity to 425.7 fb^{-1} , correspond-
69 ing to 468 million $B\bar{B}$ pairs, collected at the $\Upsilon(4S)$ resonance (on-resonance) and 45 fb^{-1} collected
70 40 MeV below the resonance (off-resonance) by the *BABAR* detector. The off-resonance events are
71 used to describe the non- $B\bar{B}$ (continuum) background. A simulated sample of $B\bar{B}$ events with
72 integrated luminosity equivalent to approximately three times the size of the data sample is also
73 used.

74 A detailed description of the *BABAR* detector and the algorithms used for charged and neutral
75 particle reconstruction and identification is provided elsewhere [7]. High-momentum particles are
76 reconstructed by matching hits in the silicon vertex tracker (SVT) with track elements in the drift
77 chamber (DCH). Lower momentum tracks, which do not leave signals on many wires in the DCH due
78 to the bending induced by the 1.5 T solenoid field, are reconstructed solely in the SVT. Charged
79 hadron identification is performed by combining the measurements of the energy deposition in
80 the SVT and in the DCH with the information from a Cherenkov detector (DIRC). Electrons are
81 identified by the ratio of the energy deposited in the calorimeter (EMC) to the track momentum, the
82 transverse profile of the shower, the energy loss in the DCH, and the Cherenkov angle in the DIRC.
83 Muons are identified in the instrumented flux return (IFR), composed of resistive plate chambers
84 and layers of iron. Muon candidates are required to have a path length and hit distribution in
85 the IFR and energy deposition in the EMC consistent with that expected for a minimum-ionizing
86 particle.

3 Event Selection and Kaon Tagging

We preselect a sample of hadronic events with at least four charged tracks. To reduce continuum background, we require that the ratio of the 2nd to the 0th order Fox-Wolfram [8] variables be less than 0.6. We then select a sample of partially reconstructed B mesons in the channel $\bar{B}^0 \rightarrow D^{*+} X \ell^- \bar{\nu}_\ell$, by retaining events containing a charged lepton ($\ell = e, \mu$) and a low momentum pion (soft pion, π_s^+) from the decay $D^{*+} \rightarrow D^0 \pi_s^+$. The lepton momentum [?] must be in the range $1.4 < p_{\ell^-} < 2.3 \text{ GeV}/c$ and the soft pion candidate must satisfy $60 < p_{\pi_s^+} < 190 \text{ MeV}/c$. The two tracks must be consistent with originating from a common vertex, constrained to the beam-spot in the plane transverse to the beam axis. Finally, we combine p_{ℓ^-} , $p_{\pi_s^+}$ and the probability from the vertex fit into a likelihood ratio variable (η), optimized to reject $B\bar{B}$ background. If more than a combination is found in an event, we keep that with the largest value of η .

Using conservation of momentum and energy, the invariant mass squared of the undetected neutrino is calculated as $\mathcal{M}_\nu^2 \equiv (E_{\text{beam}} - E_{D^*} - E_\ell)^2 - (\vec{p}_{D^*} + \vec{p}_\ell)^2$, where E_{beam} is half the total center-of-mass energy and E_ℓ (E_{D^*}) and \vec{p}_ℓ (\vec{p}_{D^*}) are the energy and momentum of the lepton (the D^* meson). Since the magnitude of the B meson momentum, p_B , is sufficiently small compared to p_ℓ and p_{D^*} , we set $p_B = 0$. As a consequence of the limited phase space available in the D^{*+} decay, the soft pion is emitted nearly at rest in the D^{*+} rest frame. The D^{*+} four-momentum can therefore be computed by approximating its direction as that of the soft pion, and parameterizing its momentum as a linear function of the soft-pion momentum. We select pairs of tracks with opposite electric charge for our signal ($\ell^\mp \pi_s^\pm$) and we use same-charge pairs ($\ell^\pm \pi_s^\pm$) for background studies.

Several processes where D^{*+} and ℓ^- originate from the same B -meson produce a peak near zero in the \mathcal{M}_ν^2 distribution. The peaking signal consists of (a) $\bar{B}^0 \rightarrow D^{*+} \ell^- \bar{\nu}_\ell$ decays (primary); (b) $\bar{B}^0 \rightarrow D^{*+} (n\pi) \ell^- \bar{\nu}_\ell$ (D^{**}), (c) $\bar{B}^0 \rightarrow D^{*+} \tau^- \bar{\nu}_\tau$, $\tau^- \rightarrow \ell^- \bar{\nu}_\ell \nu_\tau$. The main source of peaking background is due to charged- B decays to excited resonant or non resonant charm excitations, $B^+ \rightarrow D^{*+} (n\pi) \ell^- \bar{\nu}_\ell$, or to τ leptons, fake lepton cases $B \rightarrow D^{*+} h^- X$ (fake-lepton), where the hadron ($h = \pi, K, D$) is erroneously identified as, or decays to, a charged lepton. We also include radiative events, where photons with energy above 1 MeV are emitted by any charged particle, as described by PHOTOS [9] in our simulation. We define the signal region $\mathcal{M}_\nu^2 > -2 \text{ GeV}^2/c^4$, and the sideband $-10 < \mathcal{M}_\nu^2 < -4 \text{ GeV}^2/c^4$.

Light quark (continuum) events and random combinations of a low momentum pion and an opposite charge lepton from combinatorial $B\bar{B}$ events, contribute to the non-peaking background. We determine the number of signal events in our sample with a minimum χ^2 fit to the \mathcal{M}_ν^2 distribution in the interval $-10 < \mathcal{M}_\nu^2 < 2.5 \text{ GeV}^2/c^4$. In the fit, the continuum contribution is obtained from off-peak events, normalized by the on-peak to off-peak luminosity ratio, the other contributions are taken from the simulation. The amount of events from combinatorial $B\bar{B}$ background, primary decays and D^{**} are allowed to vary in the fit, while the other peaking contributions (O few percent) are fixed to the simulation expectations, rescaled by the luminosities ratios. The amount of B^0 mesons in the sample is then obtained assuming that 2/3 of the fitted amount of D^{**} events are produced by B^+ decays, as suggested by simple isospin considerations. A total of $(5370 \pm 6) \cdot 10^3$ peaking events are found; in the full range peaking events account for about 30% of the sample, continuum background for about 10%. The result of the fit is displayed in Fig.1

128

We select kaons from all the charged tracks with momentum larger than 0.2 GeV/c using a standard algorithm which combines DIRC informations with the measurements of the energy losses in the

130

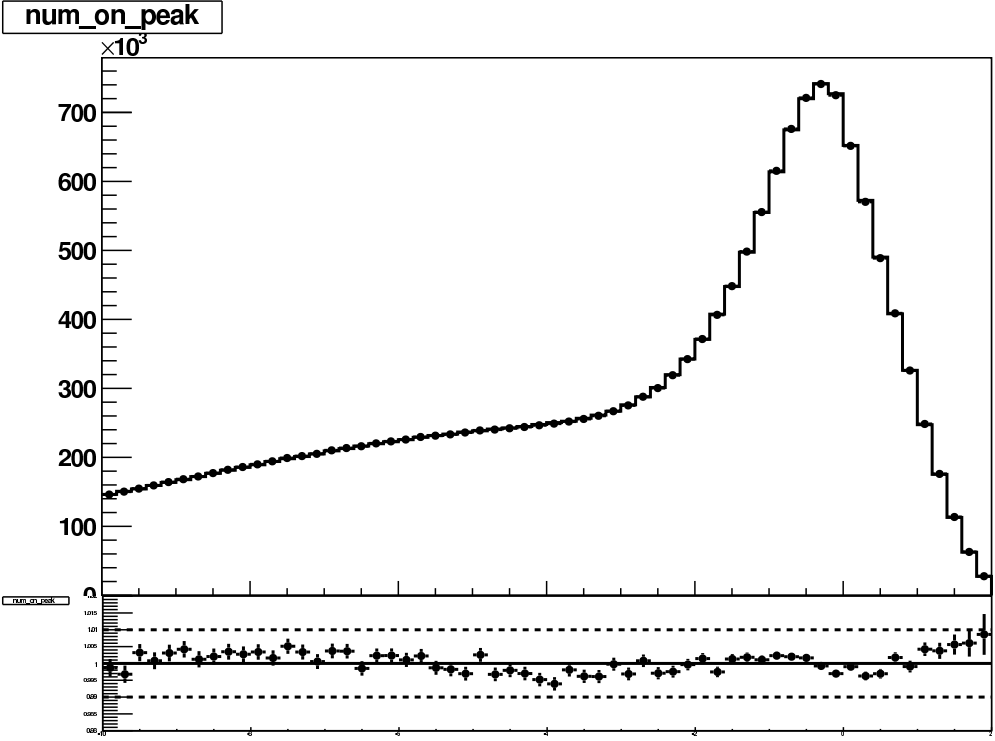


Figure 1: Top plot: \mathcal{M}_ν^2 distribution for the data, points with error bars, and the fitted contributions from signal, peaking background, $B\bar{B}$ combinatorial and rescaled off-peak events (continuous line overlaid). Bottom plot: ratio between the data and the fit result. The two dotted lines mark the $\pm 1\%$ range.

131 SVT and DCH. True kaons are identified with 86% efficiency and 3.4% pion mis-identification rate.
132 Kaons may be produced from the decay of the D^0 from the partially reconstructed B^0 (K_R), or in
133 any step of the decay of the other B (K_T).

134 We exploit the relation between the charge of the lepton and that of the K_T to tag mixing.
135 When an oscillation takes place, a K_T from a Cabibbo Favored (CF) decay has the same electric
136 charge as the ℓ . Equal-charge combinations are also observed from Cabibbo Supressed (CS) K_T
137 production in unmixed events, and from CF K_R production. Unmixed CF K_T , mixed CS K_T , and
138 CS K_R , result in opposite-charge combinations. Fake kaons contribute both to equal and opposite
139 charge events with comparable rates.

140 We distinguish K_T from K_R using proper-time difference information. We define $\Delta Z = Z_{rec} -$
141 Z_{tag} , where Z_{rec} is the projection along the beam direction of the B_{rec} decay point, and Z_{tag} is the
142 projection along the same direction of the intersection of the K track trajectory with the beam-spot.
143 In the boost approximation [10] we measure the proper-time-difference between the two B mesons
144 using the relation $\Delta T = \Delta Z / (\beta\gamma c)$, where the parameters β, γ expressing the Lorentz Boost from
145 the Laboratory to the $\Upsilon(4S)$ rest frame, are determined run by run from PEP-II settings. We reject
146 events if the error $\sigma(\Delta T)$ exceeds 3 ps.

147 Due to the short lifetime and small boost of the D^0 meson, small values of ΔT are expected
148 for the K_R . Much larger values are instead expected for CF mixed K_T , due to the long period of
149 the B^0 oscillation (about six times the B^0 lifetime). By fitting the ΔT distribution for equal and
150 opposite charge ℓ -K combinations, we also compute the contamination from CS K_T decays.

151 To improve the separation between K_T and K_R , we also exploit kinematics. The ℓ and the D^{*+}
152 are emitted at large angles in the rest frame of the decaying B^0 : therefore the angle $\theta_{\ell K}$ between
153 the ℓ and the K_R has values close to π , and $\cos(\theta_{\ell K})$ close to -1. The corresponding distribution
154 for the K_T is instead uniform.

155 If more than a Kaon is found in an event, we consider each $\ell - K$ combination in turn. We
156 use parameterized simulations (toys) to verify the effect of this choice on the computation of the
157 statistical uncertainty.

158 **4 Extraction of δ_{CP}**

159 The measurement proceeds in two steps.

160 We first measure the sample composition of the eight tagged samples divided by lepton kind,
 161 lepton charge and Kaon charge, with the fit to \mathcal{M}_ν^2 described above. We also fit the four inclusive
 162 lepton samples to determine the charge asymmetries at the reconstruction stage.

163 The results of the first stage are used in the second stage, where we fit simultaneously the $\cos\theta_{\ell K}$
 164 and ΔT distributions in the eight tagged samples. The individual $\cos\theta_{\ell K}$ shapes are obtained from
 165 the histograms of the simulated distributions for $B\bar{B}$ events, separately for K_T and K_R events. Off-
 166 peaks events are interpolated to parameterize the continuum distribution. The ΔT distributions
 167 for $K_T B\bar{B}$ events are parameterized as the convolutions of the theoretical distributions with the
 168 resolution function: $\mathcal{G}_i(\Delta T) = \int_{-\infty}^{+\infty} \mathcal{F}_i(\Delta t|\vec{\Theta})\mathcal{R}(\Delta T, \Delta t)d(\Delta t)$, where Δt is the actual difference
 169 between the times of decay of the two mesons and $\vec{\Theta}$ is the vector of the physical parameters.

170 B^+ decays are parameterized by an exponential function, $\mathcal{F}_{B^+} = \Gamma_+ e^{-|\Gamma_+ \Delta t|}$, where the B^+
 171 partial decay width is computed as the inverse of the lifetime $\Gamma_+^{-1} = \tau_+ = (1.641 \pm 0.008)$ ps.

172 B^0 decay are described by the following expressions:

$$\begin{aligned} \mathcal{F}_{\bar{B}^0 B^0}(\Delta t) &= \mathcal{E}(\Delta t) \left[\left(1 + \left| \frac{q}{p} \right|^2 r'^2 \right) \cosh(\Delta\Gamma\Delta t/2) + \left(1 - \left| \frac{q}{p} \right|^2 r'^2 \right) \cos(\Delta m_d \Delta t) - \left| \frac{q}{p} \right| (b + c) \sin(\Delta m_d \Delta t) \right] \quad (5) \\ \mathcal{F}_{B^0 \bar{B}^0}(\Delta t) &= \mathcal{E}(\Delta t) \left[\left(1 + \left| \frac{p}{q} \right|^2 r'^2 \right) \cosh(\Delta\Gamma\Delta t/2) + \left(1 - \left| \frac{p}{q} \right|^2 r'^2 \right) \cos(\Delta m_d \Delta t) + \left| \frac{p}{q} \right| (b - c) \sin(\Delta m_d \Delta t) \right] \\ \mathcal{F}_{\bar{B}^0 \bar{B}^0}(\Delta t) &= \mathcal{E}(\Delta t) \left[\left(1 + \left| \frac{p}{q} \right|^2 r'^2 \right) \cosh(\Delta\Gamma\Delta t/2) - \left(1 - \left| \frac{p}{q} \right|^2 r'^2 \right) \cos(\Delta m_d \Delta t) - \left| \frac{p}{q} \right| (b - c) \sin(\Delta m_d \Delta t) \right] \left| \frac{q}{p} \right|^2 \\ \mathcal{F}_{B^0 B^0}(\Delta t) &= \mathcal{E}(\Delta t) \left[\left(1 + \left| \frac{q}{p} \right|^2 r'^2 \right) \cosh(\Delta\Gamma\Delta t/2) - \left(1 - \left| \frac{q}{p} \right|^2 r'^2 \right) \cos(\Delta m_d \Delta t) + \left| \frac{q}{p} \right| (b + c) \sin(\Delta m_d \Delta t) \right] \left| \frac{p}{q} \right|^2 \\ \mathcal{E}(\Delta t) &= \frac{\Gamma_0}{2(1 + r'^2)} e^{-\Gamma_0 |\Delta t|}, \end{aligned}$$

173 where the first index refers to the flavor of the B_{rec} at decay time and the second to the B_{tag} .
 174 $\Gamma_0 = \tau_{B^0}^{-1}$ is the average width of the two B^0 mass eigenstates, $\Delta\Gamma$ the width difference, r' a tiny
 175 (O %) parameter resulting from the interference of CF and Doubly Cabibbo Suppressed (DCS)
 176 decays in the B_{tag} side, b and c two parameters expressing the CP violation arising from that
 177 interference [11]. In the Standard Model $b = 2r' \sin(2\beta + \gamma) \cos\delta'$, $c = -2r' \cos(2\beta + \gamma) \sin\delta'$, where
 178 β and γ are angles of the Unitary Triangle [12], and δ' is a strong phase. Besides $|q/p|$, also Δm_d ,
 179 τ_{B^0} , r' , b , and c are determined as effective parameters to reduce the systematic uncertainty. The
 180 value of $\Delta\Gamma$ is instead fixed to zero, and then varied within its allowed range when computing the
 181 systematic uncertainty.

When the K_T comes from the decay of the B^0 meson to a CP-eigenstate (as, for instance $B^0 \rightarrow D^{(*)} D^{(*)}$), a different expression applies:

$$\mathcal{F}_{CPe}(\Delta t) = \frac{\Gamma_0}{4} e^{-\Gamma_0 |\Delta t|} (1 \pm S \sin(\Delta m_d \Delta t) \pm C \cos(\Delta m_d \Delta t)),$$

182 where the sign + is used if the B_{rec} decays as a B^0 and the sign - otherwise. We take the values
 183 of S and C , and the fraction of these events in each sample (about 1%) from the simulation.

184 The resolution function $\mathcal{R}(\Delta T, \Delta t)$ accounts for the experimental uncertainties in the measure-
 185 ment of ΔT , for the smearing due to the boost approximation, and for the displacement of the K_T

186 production point from the B_{tag} decay position due to the motion of the charm meson. It consists
 187 of the superposition of several Gaussian functions convoluted with exponentials. We use a different
 188 set of parameters for peaking and for combinatoric events.

189 To describe the ΔT distributions for K_R events, $\mathcal{G}_{K_R}(\Delta T)$, we select a sub-sample of data
 190 containing less than 5% K_T decays, and we use the background subtracted histograms in our
 191 likelihood. As an alternative, we apply the same selection to the simulation and we correct the ΔT
 192 distribution predicted by the Monte Carlo by the ratio of the histograms extracted from data and
 193 simulated events. Simulation shows that the distributions so obtained are unbiased.

194 We take the average of the two δ_{CP} determinations obtained with the two different strategies
 195 as our nominal result.

196 Continuum events ($\mathcal{G}_{cnt}(\Delta T)$) are represented by a decaying exponential, convoluted with a res-
 197 olution function similar to that used for B-events. The effective lifetime and resolution parameters
 198 are determined by fitting simultaneously the off-peak data.

199 The two-dimensional PDFs are computed as the product of the ΔT and $\cos(\theta_{\ell K})$ functions.

200 We perform a binned maximum likelihood fit. Events belonging to each of the four categories
 201 are grouped in 100 ΔT bin, 25 $\sigma(\Delta T)$ bins, 4 $\cos\theta_{\ell,K}$ bins, and 5 \mathcal{M}_ν^2 bins. We further split data
 202 in five bins of K momentum, p_K , to account for the dependencies of several parameters, describing
 203 the ΔT resolution function, the $\cos(\theta_{\ell K})$ distributions, the fractions of K_T events, etc., observed
 204 in the simulation.

205 The rate of events in each bin (\vec{j}) and per each tagged sample are then expressed as the sum of
 206 the predicted contributions from peaking events, $B\bar{B}$ combinatorial and continuum:

$$\begin{aligned} \mathcal{N}_{\ell K}(\vec{j}) &= \mathcal{N}[(1 - f_{B^+} - f_{CPe} - f_{cmb} - f_{cnt})\mathcal{G}_{B^0}(\vec{j}) + f_{B^+}\mathcal{G}_{B^+}(\vec{j}) + f_{CPe}\mathcal{G}_{CPe}(\vec{j}) \\ &+ f_{cmb}^0\mathcal{G}_{B^0,cmb}(\vec{j}) + f_{cmb}^+\mathcal{G}_{B^+,cmb}(\vec{j}) + f_{cnt}\mathcal{G}_{cnt}(\vec{j})] \end{aligned} \quad (6)$$

207 where the fractions of peaking B^+ (f_{B^+}), CP eigenstates (f_{CPe}), combinatoric $B\bar{B}$ (f_{cmb}), and
 208 continuum (f_{cnt}) events in each \mathcal{M}_ν^2 interval is computed from the results of the first stage. The
 209 amounts of B^0 (f_{cmb}^0) and of B^+ events ($f_{cmb}^+ = f_{cmb} - f_{cmb}^0$) in the combinatoric background are
 210 assumed from the simulation.

211 Accounting for mistags and K_R events, the peaking B^0 contributions to the equal-charge samples
 212 are:

$$\begin{aligned} \mathcal{G}_{\ell^+K^+}(\vec{j}) &= (1 + \mathcal{A}_{rec,\ell})(1 + \mathcal{A}_{tag}) \\ &\quad \{ (1 - f_{K_R}^{++})[(1 - \omega^+)\mathcal{G}_{B^0B^0} + \omega^-\mathcal{G}_{B^0\bar{B}^0}(\vec{j})] + f_{K_R}^{++}(1 - \omega'^+)\mathcal{G}_{K_R}(\vec{j})(1 + \bar{\chi}_d\mathcal{A}_{\ell\ell}) \} \\ \mathcal{G}_{\ell^-K^-}(\vec{j}) &= (1 - \mathcal{A}_{rec,\ell})(1 - \mathcal{A}_{tag}) \\ &\quad \{ (1 - f_{K_R}^{--})[(1 - \omega^-)\mathcal{G}_{\bar{B}^0\bar{B}^0} + \omega^+\mathcal{G}_{\bar{B}^0B^0}(\vec{j})] + f_{K_R}^{--}(1 - \omega'^-)\mathcal{G}_{K_R}(\vec{j})(1 - \bar{\chi}_d\mathcal{A}_{\ell\ell}) \} \end{aligned}$$

213 where the reconstruction asymmetries are computed separately for the e and μ samples. We allow
 214 for different mistags probabilities for K_T (ω^\pm) and K_R (ω'^\pm), because the former come from a
 215 mixture of D mesons, while the others are produced by D^0 decays only.

216 The parameters $f_{K_R}^{\pm\pm}(p_k)$ describe the fractions of K_R tags in each sample. All these parameters
 217 depend of the Kaon momentum. We let the fit determine the values of the $f_{K_R}^{\pm\pm}$ parameters in every
 218 p_k bin.

219 A total of 171 parameters are determined in the fit.

220 4.1 Fit Validation

221 Several test are performed to validate our result.

222 We first analyze simulated events as the data, considering first only B^0 signal and adding step
223 by step all the other samples. At any stage, the fit reproduces the generated values of $|q/p|$ (zero),
224 and of the other most significant parameters ($\mathcal{A}_{rec,\ell}$, \mathcal{A}_{tag} , Δm_d , and τ_{B^0}).

225 We then repeat the test, randomly rejecting B^0 or \bar{B}^0 events in order to produce samples of
226 simulated events with $\delta_{CP} = \pm 0.005, \pm 0.01, \pm 0.025$. Also in this case the generated values are well
227 reproduced by the fit.

228 By removing events we also vary artificially $\mathcal{A}_{rec,\ell}$ or \mathcal{A}_{tag} , testing values in the range of $\pm 10\%$.
229 In each case the input values are correctly determined, and an unbiased value of $|q/p|$ is always
230 obtained.

231 Parameterized simulations (toys) are used to check the estimate of the result and its statistical
232 uncertainty. We perform 173 pseudo-experiments, each with the same amount of events as the
233 data. We obtain a value of the likelihood larger than the data one in 23% of the cases.

234 The distribution of the results is described by a Gaussian function with a central value biased
235 by -3.6×10^{-4} (0.4σ) wrt the nominal result. We quote this discrepancy as a systematic error
236 related to the analysis bias.

237 The pull distribution is described by a Gaussian function, with a central value -0.48 ± 0.11
238 and RMS width of 1.44 ± 0.08 . The statistical uncertainty is therefore somewhat underestimated.
239 However, by fitting the likelihood profile near the minimum with a parabola, we obtain an esti-
240 mation of the statistical uncertainty in good agreement with the RMS width of the distribution of
241 the pseudo-experiments results. Therefore we assume the likelihood profile determination as the
242 statistical uncertainty of our result.

Table 1: Breakdown of the main systematic uncertainties affecting our result

Source	Range Variation	$\Delta q/p $
Peaking Sample Composition	6.8%	$+1.15 \times 10^{-3}$ -1.49×10^{-3}
Combinatoric Sample Composition		$\pm 0.39 \times 10^{-3}$
ΔT Resolution Model		$+0.60 \times 10^{-3}$
K_R fraction		$\pm 0.11 \times 10^{-3}$
$K_R \Delta T$ distribution		$\pm 0.65 \times 10^{-3}$
Fit Bias		$+0.46 \times 10^{-3}$ -0.58×10^{-3}
CP-eigenstate description		—
Physical Parameters		$+0.28 \times 10^{-3}$
Total		$+1.60 \times 10^{-3}$ -1.78×10^{-3}

5 Systematic Uncertainties and Consistency Checks

We consider several sources of systematic uncertainties. We vary each quantity by its uncertainty, as discussed below, we repeat the measurement, and we consider the variation of the result as the corresponding systematic uncertainty; we then add in quadrature all the contributions to compute the overall systematic error.

Peaking Sample Composition: we vary the sample composition in the second stage fit by the statistical uncertainties obtained at the first stage; the corresponding variation is added in quadrature to the systematic uncertainty. We then vary the fraction of B^0 to B^+ in the D_s^{*+} peaking sample in the range $50 \pm 25\%$ to account for (large) violation of isospin symmetry. Finally we conservatively vary the fraction of CP-eigenstates by $\pm 50\%$.

$B\bar{B}$ combinatoric sample composition: the fraction of B^+ and B^0 in the $B\bar{B}$ combinatorial background is determined by the simulation. We vary this fraction by $\pm 4.5\%$, which corresponds to the error in the inclusive branching fraction $B^0 \rightarrow D^{*+} X$.

ΔT resolution model: In order to reduce the time consuming in the fit validation, all the parameters describing the resolution function are fixed to the values obtained in a previous iteration in which only the resolution is floated. We perform a fit by leaving free all the parameters and we quote the difference wrt the nominal one as systematic error.

K_R fraction: we vary the fraction of $B^+ \rightarrow K_R X$ to $B^0 \rightarrow K_R X$ by $\pm 6.8\%$, which corresponds to the uncertainty on the fraction $\frac{BR(D^{*0} \rightarrow K^- X)}{BR(D^{*+} \rightarrow K^- X)}$.

$K_R \Delta T$ distribution We add half the difference between the results obtained using the two different strategies to describe the ΔT distribution to the systematic uncertainty.

fit bias We add the statistical error on the validation test we performed with the detailed simulation and the difference between the nominal result and the central value of the pseudo-experiments ones.

CP eigenstates description We vary the S and C parameters describing the CP-eigenstates by their statistical uncertainty as obtained from simulation.

physical parameters We fixed the value of $\Delta\Gamma$ to 0.02 ps^{-1} instead of zero. The lifetime of the B^0 and B^+ mesons and the Δm_d are floated in the fit. We fixed each in turn to the world average.

By adding in quadrature all the contributions described above we compute the overall systematic uncertainty of $+1.60 \times 10^{-3}$ to -1.78×10^{-3} . Table 1 summarizes all the systematic uncertainties described above.

274 **6 Results**

275 We perform a blind analysis: the value of $|q/p|$ is kept masked until the study of the systematic
 276 uncertainties is completed and all the consistency checks are successfully accomplished; the values
 277 of all the other fit parameters, instead, are not masked.

278 We find: $\left| \frac{q}{p} \right| = 0.99971 \pm 0.00084$.

279 Figures 2 and 3 show the fit projections for ΔT in linear and logarithmic scale, respectively.
 280 Figure 4 shows the fitted $\cos\theta_{\ell K}$ distribution.

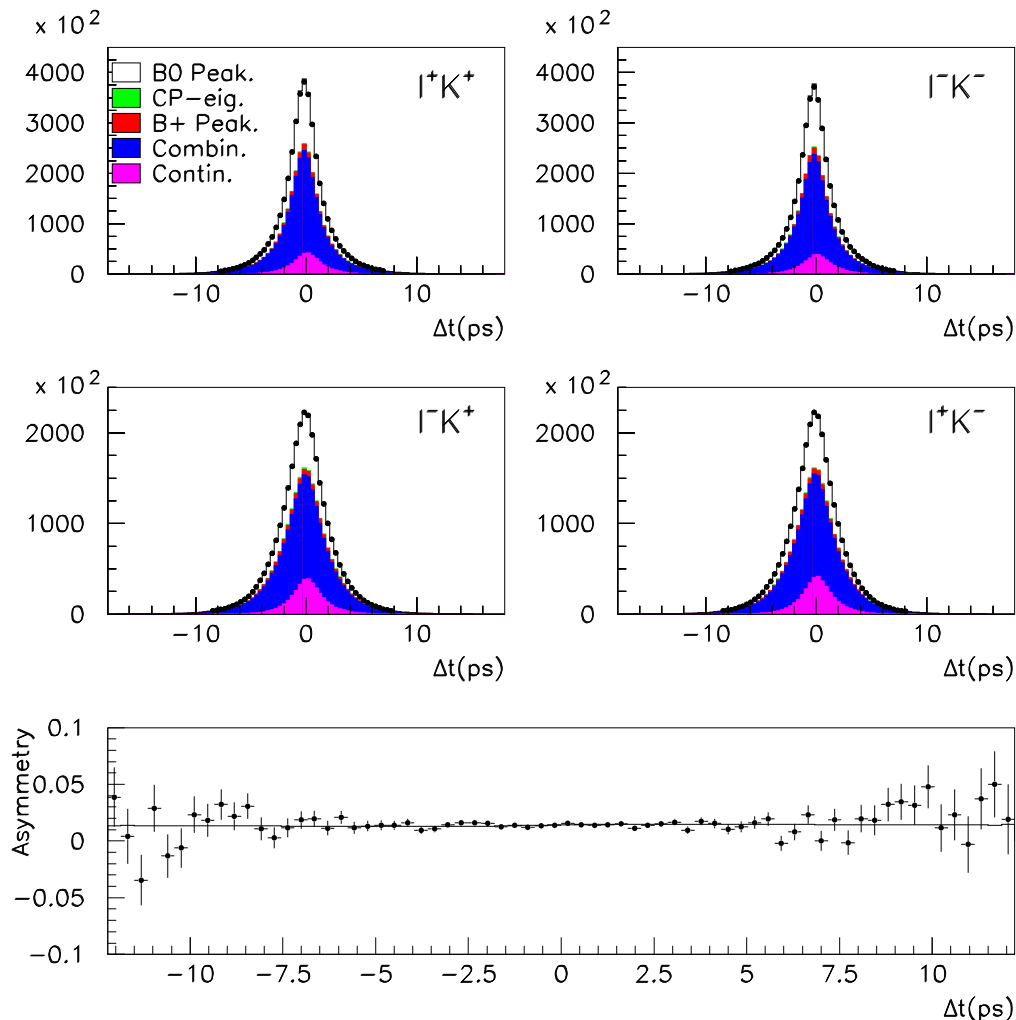


Figure 2: ΔT distribution for the data, point with error bars, and the fitted contributions from signal, peaking B^+ background, CP-eigenstates, $B\bar{B}$ combinatorial and continuum events. Top left plot: $\ell^+ K^+$. Top right plot: $\ell^- K^-$. Central left plot: $\ell^- K^+$ events. Central right plot: $\ell^+ K^-$ events. Bottom plot: Raw asymmetry between $\ell^+ K^+$ and $\ell^- K^-$ events.

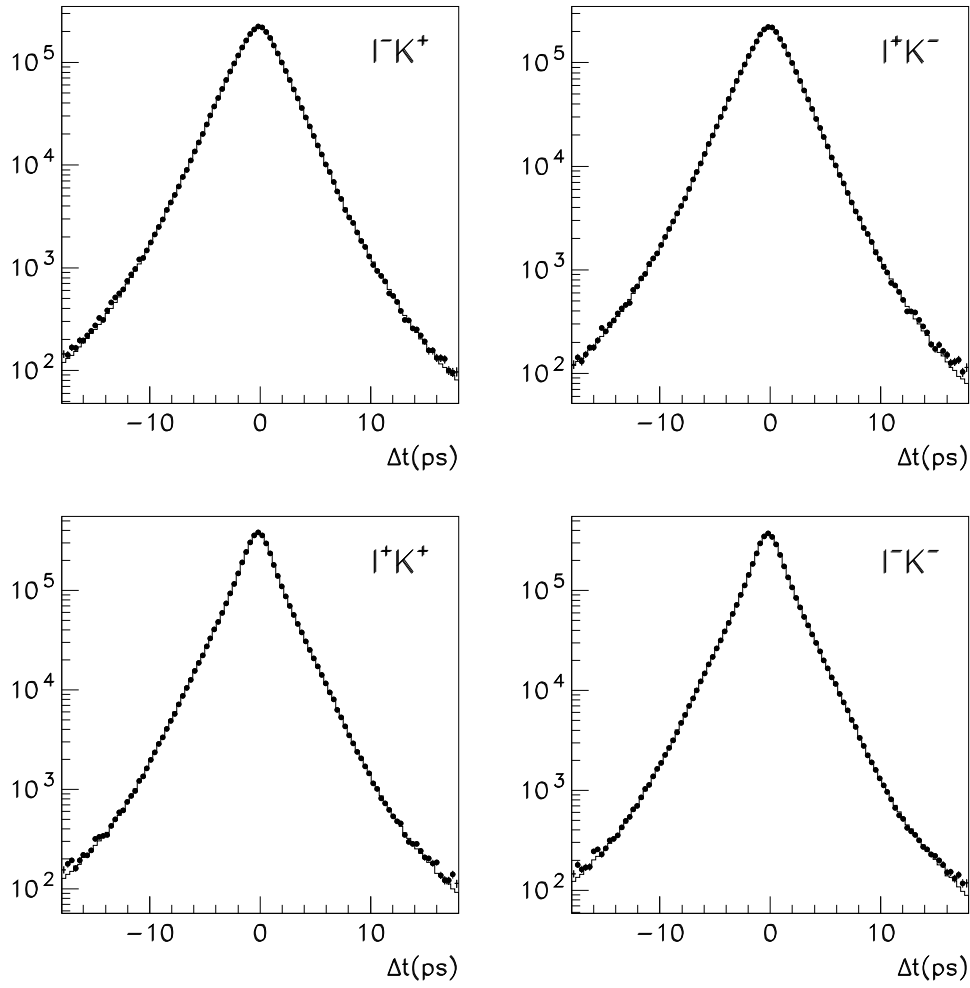


Figure 3: Same as Fig. 2 with logarithmic scale.

282

283

284

We report on Tab. 2 the fit results for the most significant parameters.

285

286

287

The values of Δm_d is well consistent with the world average, so proving that the ΔT distributions are well understood. The value of τ_{B^0} is, on the contrary, somewhat biased. By fixing its value to

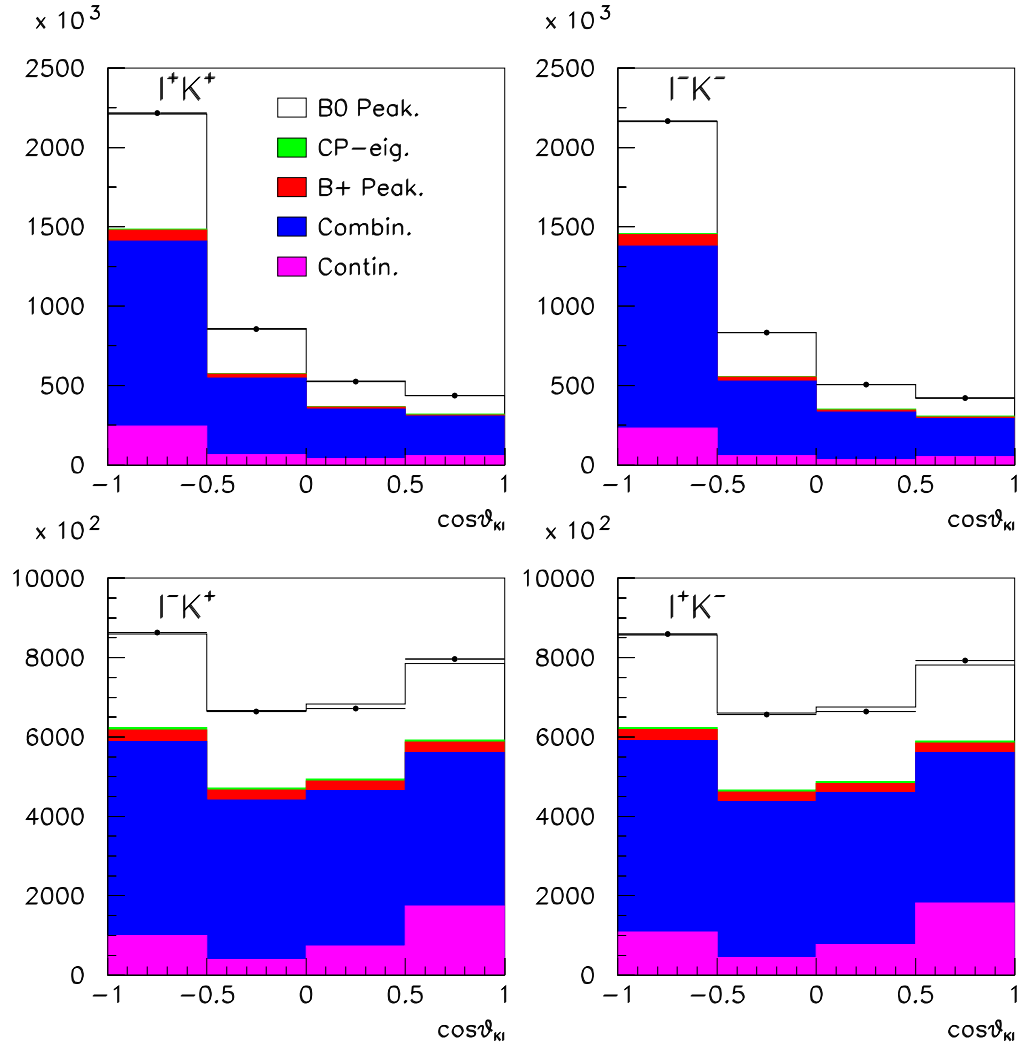


Figure 4: $\cos\theta_{\ell K}$ distribution for the data, point with error bars, and the fitted contributions from signal, CP-eigenstates, peaking B^+ background, $B\bar{B}$ combinatorial and continuum events. Top left plot: $\ell^+ K^+$. Top right plot: $\ell^- K^-$. Central left plot: $\ell^- K^+$ events. Central right plot: $\ell^+ K^-$ events.

Table 2: Results: second column, fit to the data; third, fit to simulated events; last : values of the parameters in the simulation at generation stage

Parameter	Fit to the data	Fit to the simulation	MC truth
$ q/p $	0.99971 ± 0.00084	0.99965 ± 0.00046	1
$\mathcal{A}_{rec,e}$	0.0030 ± 0.0004	0.0097 ± 0.0002	
$\mathcal{A}_{rec,\mu}$	0.0031 ± 0.0005	0.0084 ± 0.0003	
\mathcal{A}_{tag}	0.0137 ± 0.0003	0.0147 ± 0.0001	
τ_{B^0}	1.5535 ± 0.0019	1.5668 ± 0.0012	1.540
Δm_d	0.5085 ± 0.0009	0.4826 ± 0.0006	0.489

288 the world average, the $|q/p|$ result increases by 0.18×10^{-3} . This effect is taken into account in the
 289 systematic error computation.

290 A sizable asymmetry is observed at the reconstruction stage, for both e and μ , and at the
 291 K tagging stage, as also observed in the simulation. This hints that the main sources of charge
 292 asymmetry are due to the reconstruction of the π_s and the K .

293 7 Conclusions

We present a new precise measurement of the parameter governing CP violation in $B^0 \bar{B}^0$ os-
 cillations. With a technique based on partial $\bar{B}^0 \rightarrow D^{*+} \ell^- \bar{\nu}_\ell$ reconstruction and K tagging we
 find

$$\left| \frac{q}{p} \right| = 0.99971 \pm 0.00084^{+0.00160}_{-0.00178},$$

where the first uncertainty is statistical and the second is systematic. The corresponding value of
 the dilepton asymmetry,

$$\mathcal{A}_{\ell\ell} = (0.06 \pm 0.17^{+0.32}_{-0.36})\%,$$

294 is well consistent with and more precise than the results from dilepton measurements. No deviation
 295 is observed from the SM expectation [13].

296 References

- 297 [1] M. Ciuchini *et al.*, J. High Energy Phys. 0308, 031 (2003).
- 298 [2] E. Nakano *et al.* (Belle collaboration), Phys. Rev. D73, 112002 (2006).
- 299 [3] B. Aubert *et al.* (BABAR collaboration), Phys. Rev. Lett. 96, 251802 (2006).
- 300 [4] V. M. Abazov *et al.* (D0 collaboration), Phys. Rev. D84, 052007 (2011).
- 301 [5] The LHCb collaboration, LHCb-CONF-2012-022 (2012).
- 302 [6] J. Beringer *et al.*, (Particle Data Group), Phys. Rev. D86, 010001 (2012).
- 303 [7] B. Aubert *et al.* (BABAR collaboration), Nucl. Instr. and Meth. in Phys. Res. A479, 1 (2002).
- 304 [8] G. C. Fox and S. Wolfram, Phys. Rev. Lett. 41, 1581 (1978).
- 305 [9] E. Barberio, B. van Eijk, and Z. Was, Comput. Phys. Commun. 66, 115 (1991); E. Barberio
306 and Z. Was, Comput. Phys. Commun. 79, 291 (1994).
- 307 [10] The BABAR Physics Book, SLAC Report SLAC-R-504.
- 308 [11] O. Long *et al.* Phys. Rev. D68, 034010 (2005).
- 309 [12] A. A. Logunov *et al.*, Phys. Lett. B 24, 181 (1967); K. G. Chetyrkin and N. V. Krasnikov,
310 Nucl. Phys. B119, 174 (1977); K. G. Chetyrkin *et al.*, Phys. Lett. B 76, 83 (1978).
- 311 [13] A. Lenz, arXiv:1205.1444.